Advances in Military Technology
Vol. 17, No. 1, 2022, pp. 47-62
ISSN 1802-2308, eISSN 2533-4123
DOI 10.3849/aimt.01520

Synthetic Aperture Radar Active Decoy

S. A. Elgamel* and M. S. Abdel-Latif

Military Technical College, Cairo, Egypt

The manuscript was received on 19 July 2021 and was accepted after revision for publication as research paper on 5 April 2022.

Abstract:

Synthetic aperture radar (SAR) has been widely involved in military reconnaissance and detection of moving targets. SAR active decoy can generate deceptive jamming signal and it can severely affect the content of SAR focused image. SAR range Doppler algorithm (RDA) is considered as one of the most common algorithms utilized in the image formation processor (IFP) in SAR sensors. In this paper, the inverse RDA (IRDA) deception jamming technique and its evaluation criteria on SAR are demonstrated. Mathematical formulations for SAR RDA with and without deception jamming are presented. Matlab simulation and results of SAR RDA under the proposed deception scenario are discussed. SAR point target simulation of the proposed deceptive jamming and false target insertion into real large scene are also introduced. Comparison of the proposed deceptive jamming to signal power ratio (JSR) required to counter SAR with other SAR jamming techniques is analyzed.

Keywords:

deception jamming, inverse range Doppler algorithm, SAR

1 Introduction

Synthetic aperture radar (SAR) has been involved in military applications such as high resolution imaging, battlefield surveillance, and moving target detection [1]. The range Doppler algorithm (RDA) is considered as one of the most well-known SAR digital processing algorithms. The RDA achieves high efficiency in both range and azimuth directions for frequency domain operations. The RDA works separately in the two dimensions depending on the time scale differences of the two-dimensional details using the range cell migration correction (RCMC) [2]. SAR served as an effective electronic support measure (ESM) in the last decade. Thus, electronic warfare (EW) researchers have been working to reduce its effectiveness and impact in this field.

Electronic counter measures (ECM) varied from traditional methods that require high jamming power to smart methods that require less jamming power. One of these smart

* *Corresponding author: Electronic Warfare Department, Military Technical College, Kobri-Elkobba, Cairo, Egypt. Phone: +20 2 2621908, E-mail: elgamel@mtc.edu.eg. ORCID 0000-0003-0627-5729.*

methods is the active decoy that is deceiving SAR using a coherent generated deceptive jamming signal [3]. The deceptive jamming principle on SAR depends on introducing a spurious scene or target on its image. The deceptive jamming signal should have the same kinematic, antenna, and signal parameters of the SAR return echo from the protected area. These SAR parameters are obtained based on collaborative receivers [4].

In [5], an effective jamming technique against SAR called multiplicative noise jamming is introduced. This technique is proposed for jamming narrow strips or small extended areas and targets. The mathematical model of this jamming technique is presented and analyzed. The noise to SAR bandwidth ratio (NSBR) controls the effect of the proposed jamming technique on the SAR output image. In [6], a mathematical model and illustration of the convolution noise jamming technique at the SAR sensor is introduced. Two parameters are proposed to control the convolution noise jamming effect on the output image of SAR sensor. These parameters are noise to SAR pulse width ratio (NSPR) and noise to synthetic time ratio (NSTR). Controlling both NSPR and NSTR allows the possibility to determine the coverage of the convolution noise jamming on the output image of SAR, which consequently allows smart use of the power to produce high intensity noise strips or patches to cover specific target area rather than covering the whole scene. In [7], a novel jamming technique is proposed to generate effective jamming against SAR to protect multiple displaced targets given availability of limited jamming power, which is a typical situation. This technique utilizes, in its core, the convolution noise jamming which has proven to allow high level of controllability. A closed form of the multichannel convolution noise jamming (MC-CNJ) which governs the effect on the SAR receiver is introduced. Through the proposed technique, a high intensity noise patches are formed to skin limited areas instead of scattering the jamming power over the whole SAR image. In [8], a comparative study of the performance of the deceptive and the noise jamming on a SAR focused image, with and without jamming, is performed. Structural similarity index measure (SSIM) and correlation coefficient (CC) are used as evaluation criteria to measure different jamming techniques' effect on a real SAR focused image (object of high interest). In [9],echo simulation of active deception jamming based on jammer systematic function is proposed. Matlab is used to verify simulation of point targets and real scene of the SAR active deception jamming. The simulation results show that the method is suitable for many kinds of disturbed simulation on SAR active deception, such as single-point target, multi-points target, area target, distributed target and real scene**.**

In this paper, a proposed deceptive jamming technique against monostatic SAR RDA focused image is discussed. A comparison of the proposed deceptive jamming to signal power ratio (JSR) required to counter SAR with other SAR jamming techniques is analyzed. Matlab simulations are used to demonstrate different scenarios for the proposed deception jamming technique.

This paper presents SAR deception and its evaluation criteria in section 2. RDA SAR under the proposed deception jamming and its mathematical formulation are presented in section 3. In section 4, Matlab simulation and results of SAR under different deception scenarios and a comparison of different jamming power (including the proposed deception jamming technique) required to counter SAR are discussed. Section 5 concludes this paper.

2 SAR Deception and Its Evaluation Criteria

2.1 SAR Different Structures and Operational Modes

SAR is configured with different structures, such as monostatic, bistatic, or multistatic. Monostatic SAR uses the same antenna for signal transmission and reception [10]. Since it is used in remote sensing applications, it will be considered in this paper.

SAR has three different operation modes. In the strip map mode (the first mode), the SAR antenna moves in the path parallel to the ground swath that is imaged with fixed aspect and grazing angles. In the spot light mode (the second mode), the SAR antenna continues steering the aspect angle over the synthetic path to keep looking at the same ground swath in order to get high resolution images but with smaller swath. In the scan mode (the third mode), the SAR scans its angle to cover wider ground swathes equivalent to multiple side-by-side footprints on the expense of azimuth resolution compared to strip map and spotlight modes. The strip map SAR mode is widely applied in the tactical imaging for surveillance of large ground areas scene. It gives larger images with sufficient azimuth resolution. Therefore, it will be considered in this paper.

2.2 SAR Deception Jamming Principle

The SAR deceptive jamming principle depends on introducing a spurious scene or target on its image. SAR RDA deceptive jamming inserts a certain object into the SAR focused image with a previously predetermined data such as: the objects' location, shape, size, and signal to noise power ratio (SNR). In the proposed deceptive jamming technique, the deceptive jamming parameters and the spurious image are changed from case to case depending on the SAR focused image of the protected area. For example, if the protected area is a military airport, the spurious objects may contain military airplanes, airstrips, hangars, etc. Similarly, if the protected area is a nuclear plant energy, the spurious objects may be nuclear reactors, houses for the workers, etc.

Let us assume that the SAR flies in a straight path and subjected to the geometric parameters, as shown in Fig. 1. The SAR received signal, $S_0(\tau, \eta)$ and $R(\eta)$ is the SAR instantaneous slant range. The jammer should be placed inside the protected area, where θ_j is the jamming beam slant angle and $R_j(\eta)$ is the jammer instantaneous slant range.

2.3 Deception Jamming Evaluation Criteria

Taking into consideration the SAR jamming principle, the jamming effect can be evaluated using three evaluation criteria, i.e. structural similarity index measure (SSIM) [6, 11, 12], mean absolute difference (MAD) [13, 14], and correlation coefficient (CC) [15]. In digital image processing, MAD is a measure of the similarity between image blocks.

MAD is calculated by taking the absolute difference between each pixel in the original block and the corresponding pixel in the block being used for comparison. Thus, MAD can be used as deception jamming effect evaluation criterion comparing SAR focused image with and without the deceptive jamming. MAD between the two images (with and without the deceptive jamming) is expressed as [13, 14]:

$$D_M = \sum_{i=1}^{m} \sum_{j=1}^{n} \left| f_{ij} - g_{ij} \right| \tag{1}$$

where f_{ij}, and g_{ij} are the Gray-level values of the i^{th} row, j^{th} column of pixels of the two images before and after being jammed, respectively, m and n are numbers of rows and

columns of the pixels, respectively. Thus, if there is no jamming, the two images of the protected area (with and without jamming) remain the same and $D_M = 0$ (the minimum value). However, if the jamming signals success to change the Gray-level values of the pixels, then $D_M > 0$, and the greater change, the larger the value of D_M. Therefore the value of D_M reflects the difference of the two images with and without jamming.

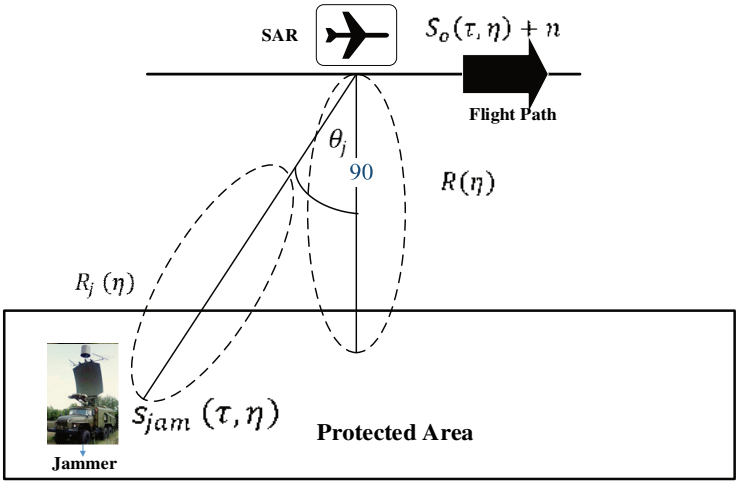

Fig. 1 SAR jamming geometric configuration

3 RDA SAR under the Proposed Deception Jamming

3.1 SAR RDA without Jamming

Fig. 2 demonstrates SAR processing steps through SAR RDA blocks. There are three major operations of the RDA algorithm (dashed line blocks): range compression, RCMC, and azimuth compression. The range compression operation is done by performing a range FFT for the raw data and then it is multiplied with a range-matched filter. The range compression is followed by range IFFT. The same processes are repeated for the azimuth compression operation and it is followed by azimuth IFFT. RCMC is performed in the range Doppler domain; it is a range time and azimuth frequency dependent.

As shown in Fig. 2, the basic processing steps of RDA are depicted and its mathematical formulations are seen in the next equations. It is considered to be operating in low squint case, i.e. squint angle = 0° [2].

The SAR received signal $S_0(\tau, \eta)$ from a point target is expressed as [16]:

$$S_0(\tau,\eta) = A_0\,\omega_r\left[\tau - 2R(\eta)\right] w_a(\eta-\eta_c)\exp\left[\begin{matrix}-\mathrm{j}4\pi f_0 R(\eta)/c + \\ +\mathrm{j}\pi K_r\left[\tau - 2R(\eta)/c\right]^2\end{matrix}\right] \qquad (2)$$

where A_0 is an arbitrary complex constant, τ is the time delay related to range dimension, η is the azimuth time referenced to closest approach, η_c is the beam center offset time, $\omega_r(\tau)$ is the range envelope (rectangular function), $w_a(\eta)$ is the azimuth envelope (sinc squared function), f_0 is the SAR center frequency, K_r is the range chirp FM rate, $R(\eta)$ is the instantaneous slant range, j is the imaginary number, and c is the microwave propagation speed. The output signal of range-matched filter $S_{rc}(\tau, \eta)$ is expressed as:

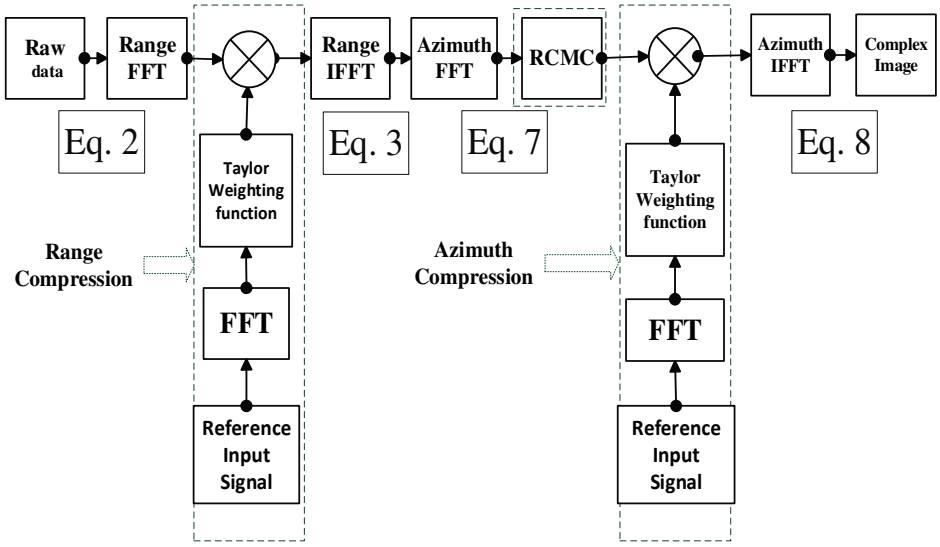

Fig. 2 Functional block diagram of basic RDA

$$S_{\mathrm{rc}}(\tau,\eta) = \mathrm{IFFT}_{\tau}\left[S_0(f_\tau,\eta)H_m(f_\tau)\right] \approx$$
$$\approx A_0\, p_{\mathrm{r}}\left[\tau - \frac{2R(\eta)}{c}\right] w_{\mathrm{a}}(\eta-\eta_{\mathrm{c}}) \exp\left(-\frac{\mathrm{j}4\pi f_0 R(\eta)}{c} - \mathrm{j}\pi\frac{2V_{\mathrm{r}}^2}{\lambda R_0}\eta^2\right) \tag{3}$$

where $p_{\mathrm{r}}(\tau)$ is the compressed pulse envelope that is the IFFT of the window and for a rectangular pulse $p_{\mathrm{r}}(\tau)$ is a sinc function, the instantaneous slant range $R(\eta) = \sqrt{R_0^2 + V_{\mathrm{r}}^2\eta^2}$, R_0 is the slant range of the closest approach, λ is the received signal wave length, and V_{r} is SAR plat form speed. The azimuth time η is referenced to zero plane for this target. The combined filter $H_m(f_\tau)$ can be written as:

$$H_m(f_\tau) = \exp\left\{\mathrm{j}\pi f_\tau^2\left[\frac{1}{K_{\mathrm{r}}} - \frac{1}{K_{\mathrm{src}}(R_0,f_\eta)}\right]\right\} \tag{4}$$

where

$$K_{\mathrm{src}}(R_0,f_\eta) = \frac{2v_{\mathrm{r}}^2 f_0^2 D^3(f_\eta,V_{\mathrm{r}})}{cR_0 f_\eta^2} \tag{5}$$

And D is the square root factor, where

$$D^2(f_\eta,V_{\mathrm{r}}) = 1 - \frac{c^2 f_\eta^2}{4V_{\mathrm{r}}^2 f_0^2} \gg \left|\frac{2f_\tau}{f_0} + \frac{f_\tau^2}{f_0^2}\right| \tag{6}$$

The signal after the azimuth FFT is expressed by

$$S_{\mathrm{az}}(\tau,f_\eta) = \mathrm{FFT}_{\eta}\left[s_{\mathrm{rc}}(\tau,\eta)\right]$$
$$= A_0\, P_{\mathrm{r}}\left(\tau - \frac{2R_0}{c}\right) W_{\mathrm{a}}(f_\eta - f_{\eta\mathrm{c}}) \exp\left(-\mathrm{j}\frac{4\pi f_0 R_0}{c} + \mathrm{j}\pi\frac{f_n^2}{K_{\mathrm{a}}}\right) \tag{7}$$

where K_a is defined from relationship between the azimuth frequency and the time as $f_\eta = -K_a\eta$, and $W_a(f_\eta - f_{\eta c})$ is the azimuth beam pattern in frequency domain. The complex image output $S_{ac}(\eta, \tau)$ after performing IFFT is expressed as:

$$S_{ac}(\eta,\tau) = A_0 P_r\left(\tau - \frac{2R_0}{c}\right) P_a(\eta) \exp\left(-j\frac{4\pi f_0 R_0}{c} + j2\pi f_{\eta c}\eta\right) \quad (8)$$

where P_a is the amplitude of the azimuth impulse response, it is a sinc function, similar to P_r, and these envelopes shows that the target is now positioned at $\tau = 2R_0/c$, and $\eta = 0$, given that η is relative to the time of the closest approach at zero Doppler position for the given target.

3.2 The Proposed Jamming Technique

The deception jamming scenario and the evaluation of the jamming effect block diagram is shown in Fig. 3. The SAR signal is intercepted and its parameters are considered to be estimated (by the ESM part of the jamming station and Air defence system). This signal is added to the SAR return echo at the SAR receiver front end. The deceptive jamming signal is transmitted with different values of JSR. The proposed jamming algorithm performs two decompression processes to generate the SAR deceptive jamming signal: azimuth and range decompression, respectively [17]. The azimuth decompression is performed by multiplying the azimuth decompression filter in each azimuth column of the signal. Similarly, the range decompression process is made by multiplying the range decompression filter in each range column of the signal, as illustrated in Fig. 4 (dashed block in Fig. 3).

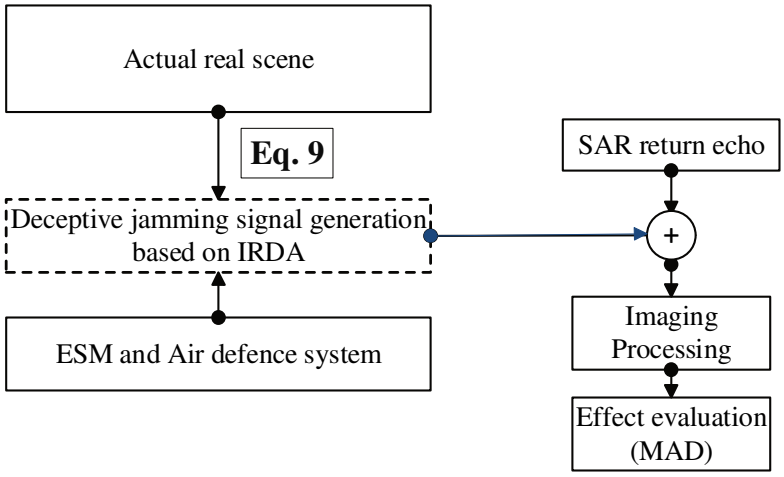

Fig. 3 Deceptive jamming scenario and its evaluation effect

The generated signal from a spurious scene or a synthesized image $s_{si}(\eta, \tau)$ is given by:

$$s_{si}(\eta,\tau) = A_j P_r\left(\tau - \frac{2R_{j0}}{c}\right) P_a(\eta) \exp\left(-j\frac{4\pi f_0 R_0}{c}\right) \exp\left(j2\pi f_{\eta c}\eta\right) \quad (9)$$

where $P_r(\tau)$ is the compressed pulse envelope, $P_a(\eta)$ is the amplitude of the impulse response of the azimuth, R_{j0} is the jammer slant range of the closest approach.

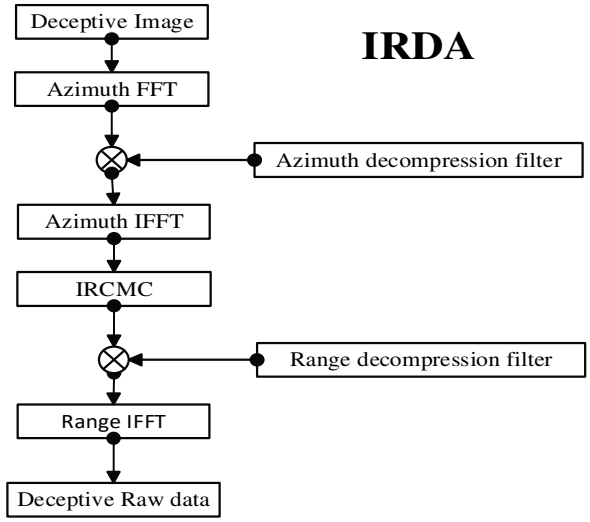

Fig. 4 Deceptive jamming signal generation based on IRDA

The required deceptive jamming raw data signal $s_{\text{jam}}(\tau, \eta)$ is obtained by performing an IFFT in both azimuth and range dimensions on the output of the range decompression filter, as following:

$$s_{\text{jam}}(\tau,\eta) = \text{IFFT}_{\tau,\eta}\left[S_{\text{rdc}}\left(f_\tau, f_\eta\right)\right] \tag{10}$$

Thus,

$$s_{\text{jam}}(\tau,\eta) = A_{\text{j}} w_{\text{r}}\left[\tau - \frac{2R_{\text{j}}(\eta)}{c}\right] w_{\text{a}}(\eta-\eta_{\text{c}}) \exp\left[\begin{matrix} -\text{j}4\pi f_0 \dfrac{R_{\text{j}}(\eta)}{c} \\ +\text{j}\pi K_{\text{r}}\left(\tau - \dfrac{2R_{\text{j}}(\eta)}{c}\right)^2 \end{matrix}\right] \tag{11}$$

For the jammer has a slant angle θ_{j}, then

$$R_{\text{j}}(\eta) = \sqrt{R_{\text{j0}}^2 + v^2\eta^2 - 2R_{\text{j0}} v\eta \sin\theta_{\text{j}}} \tag{12}$$

The SAR return echo is given by

$$s_0(\tau,\eta) = A_{\text{r}} w_{\text{r}}\left[\tau - \frac{2R_{\text{s}}(\eta)}{c}\right] w_{\text{a}}(\eta-\eta_{\text{c}}) \exp\left[\begin{matrix} -\text{j}4\pi f_0 \dfrac{R_{\text{s}}(\eta)}{c} \\ +\text{j}\pi K_{\text{r}}\left(\tau - \dfrac{2R_{\text{s}}(\eta)}{c}\right)^2 \end{matrix}\right] + n(\tau,\eta) \tag{13}$$

where A_r is the arbitrary complex constant related to the SAR return echo and $n(\tau, \eta)$ is the SAR internal noise. The received signal at the front end of the SAR with jamming is given by

$$s_{\text{rec}}(\tau,\eta) = s_{\text{j}}(\tau,\eta) + \left[s_0(\tau,\eta) + n(\tau,\eta)\right] \tag{14}$$

By substituting from Eqs (11) and (13) into (14), the received signal is given by

$$s_{\text{rec}}(\tau,\eta) = A_{\text{j}} w_{\text{r}}\left[\tau - \frac{2R_{\text{j}}(\eta)}{c}\right] w_{\text{a}}(\eta-\eta_{\text{c}}) \exp\left[\begin{array}{l} -\text{j}4\pi f_0 \dfrac{R_{\text{j}}(\eta)}{c} + \\ \text{j}\pi K_{\text{r}}\left(\tau - \dfrac{2R_{\text{j}}(\eta)}{c}\right)^2 \end{array}\right] + \\ + A_{\text{r}} w_{\text{r}}\left[\tau - \frac{2R_{\text{s}}(\eta)}{c}\right] w_{\text{a}}(\eta-\eta_{\text{c}}) \exp\left[\begin{array}{l} -\text{j}4\pi f_0 \dfrac{R_{\text{s}}(\eta)}{c} + \\ \text{j}\pi K_{\text{r}}\left(\tau - \dfrac{2R_{\text{s}}(\eta)}{c}\right)^2 \end{array}\right] + n(\tau,\eta) \tag{15}$$

If the jammer is coincident with the protected object ($\theta_{\text{j}} = 0$), so $R_{\text{s}}(\eta) = R_{\text{j}}(\eta) = \sqrt{R_{\text{jo}}^2 + v^2\eta^2}$, and the received signal is given by

$$s_{\text{rec}}(\tau,\eta) = \left(A_{\text{j}} + A_{\text{r}}\right)\left\{\begin{array}{l} w_r\left[\tau - \dfrac{2R_{\text{j}}(\eta)}{c}\right] w_{\text{a}}(\eta-\eta_{\text{c}}) + \\ \exp\left[-\text{j}4\pi f_0 \dfrac{R_{\text{j}}(\eta)}{c} + \text{j}\pi K_{\text{r}}\left(\tau - \dfrac{2R_{\text{j}}(\eta)}{c}\right)^2\right] \end{array}\right\} + n(\tau,\eta) \tag{16}$$

4 Matlab Simulation and Results of SAR

SAR Matlab simulation is considered to work in strip-map mode, and its platform flies in a straight path. All the following simulation studies are performed in SAR SNR equal to 0 dB and JSR vary [−8:8] dB. SAR considered parameters are listed in Tab. 1.

4.1 Point Target Simulation of SAR

Fig. 5 shows the received signal from a single point target. Different SAR processes are performed (after acquiring the data of SAR return echo) to focus the image. Fig. 5a depicts the raw data of a point target of SAR signal, as in (2) located at pixels (370, 325). These raw data is multiplied with the range reference function, generated as in (3) to have the results shown in Fig. 5b. Then, the azimuth reference function in (8) is created with the SAR parameters defined in Tab. 1. Thus the azimuth compression process is performed and the data can be plotted again as shown in Fig. 5c.

Tab. 1 SAR parameters

Parameter	Value
Carrier frequency	10 GHz
Chirp pulse duration	3 μs
Transmitted bandwidth	200 MHz
Pulse repetition frequency (PRF)	1.5 kHz
Effective antenna dimension along azimuth direction (L_{a})	0.5 m
Effective antenna dimension along range direction (L_{r})	0.2 m
SAR platform moving speed	250 m/s
SAR height	1.4 km

4.2 Point Target Deception Jamming against SAR

In point target deception jamming against simulation, the SAR target is considered as a point target signal as in (2). While another deceptive point target signal, as in (11), is added to SAR point target and it acts as a spurious target. Fig. 6a shows the deceptive jamming signal raw data of point target in a SAR focused image with (N_a = 512, N_r = 512). The location of the deceptive point target in the SAR image plot is considered at (256, 256). The jamming process adds another spurious target into SAR image. Fig. 6b shows the total received signal at SAR receiver front end after adding the proposed deceptive jamming, as in (15). The range compression process is performed, on the total received signal at SAR receiver front end and the result is shown in Fig. 6c. Two targets are displayed in the SAR focused image: the original point target located in pixel (N_a = 512, N_r = 512) and the spurious point target located in pixel (256, 256) of the image as shown in Fig. 6d.

MAD, as described before, is used to evaluate the difference between the two images with and without jamming. The MAD values (as an evaluation criterion) at different JSR values are listed in Tab. 2. It is shown that the higher JSR, the higher MAD.

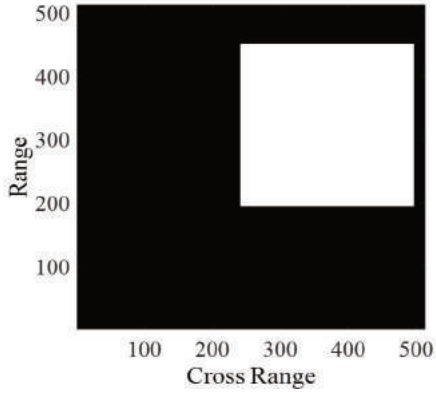

(a) Raw data

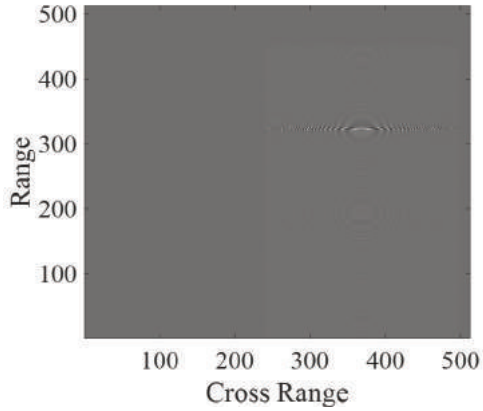

(b) Data after range compression

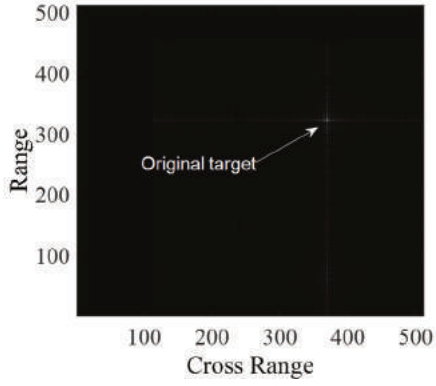

(c) Data after Azimuth compression.

Fig. 5 Point target simulation for SAR processes

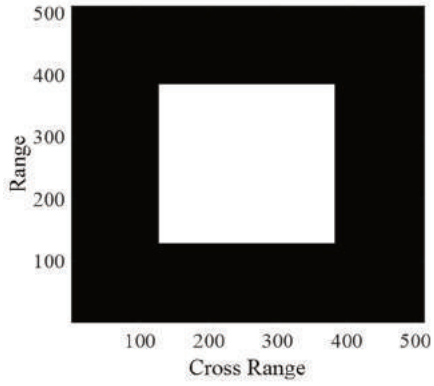

(a)The raw data of the jamming signal

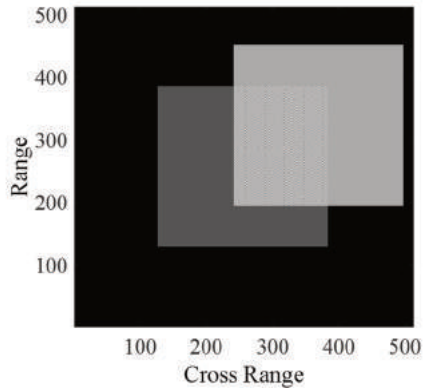

(b) The total received signal at SAR receiver front end

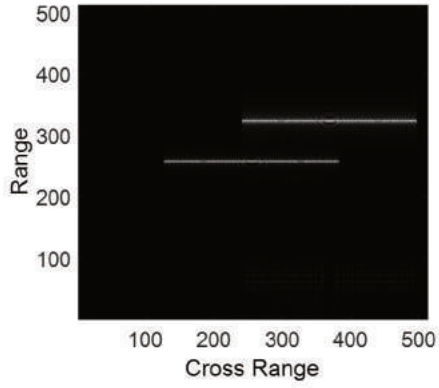

(c) Data after range compression for the total received signal

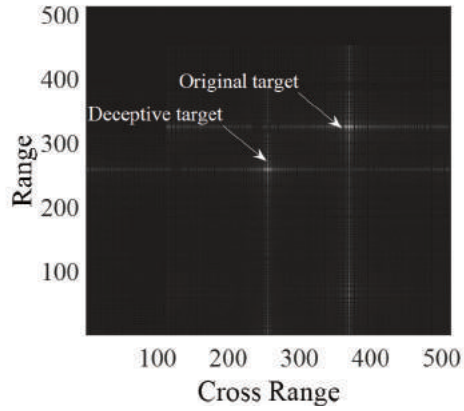

(d) SAR image plot after deception jamming

Fig. 6 Point target deceptive jamming simulation

Tab. 2 Evaluation of deceptive jamming effect of point target deception

JSR [dB]	−8	−5	−3	0	3	5	8
MAD	155.3	312.2	413.1	689.6	1 086.8	1 351.9	1667.7

4.3 False Target Insertion into Real Large Scene

In this section, the proposed deceptive jamming technique against SAR focused image (real scene) is discussed. In Fig. 7, the raw data refers to an area in the north coast of Scotland, UK (this raw data is provided by the UK defense center) [18]. It is required to insert an object into this protected area. This object is chosen to be rectangular shape and it works as the deceptive runway to form the spurious image. It is required to determine the location, size, and visibility (which is related to JSR) of the inserted object (rectangular shape).

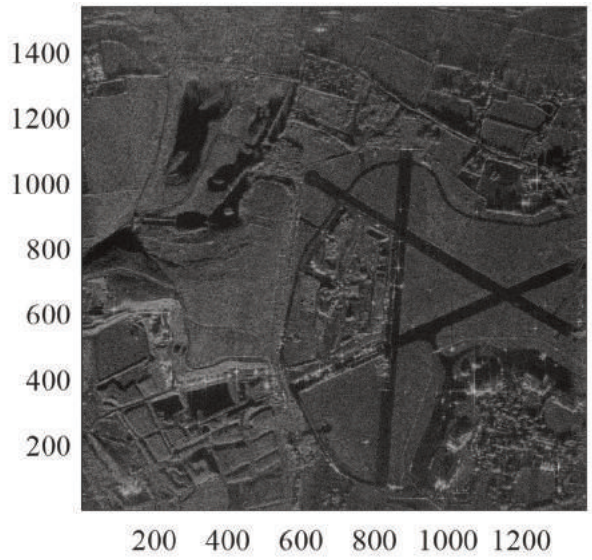

Fig. 7 Area to be protected

Fig. 8a shows a deceptive vertical rectangle object centered is inserted into SAR focused image at the location of (N_a = 1 000, N_r = 700). The parameters of the deceptive jamming deceptive target are listed in Tab. 3.

Tab. 3 Deceptive jamming signal parameters

Parameter	**Value**	**Unit**
Na	1 375	samples
Nr	1 536	samples
JSR	[−8:8]	dB
Inserted object shape	rectangle	36 × 360 samples

In Fig. 8b, a deceptive horizontal rectangle object centered at the location of (N_a = 1 150, N_r = 900) is inserted into SAR focused image. It is clear that both of the location and size of the inserted object are controlled. The MAD values at different values of JSR are listed in Tab. 4.

Tab. 4 Evaluation of jamming effect of false target insertion into large scene

JSR [dB]	−8	−5	−3	0	3	5	8
MAD	50.3	62.8	76.2	110.7	1 304.9	1 557.9	1 875.9

DOI 10.3849/aimt.01520

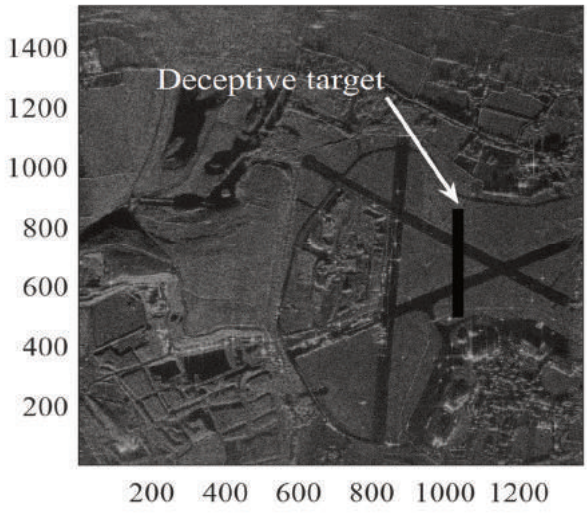

(a) A deceptive vertical rectangle

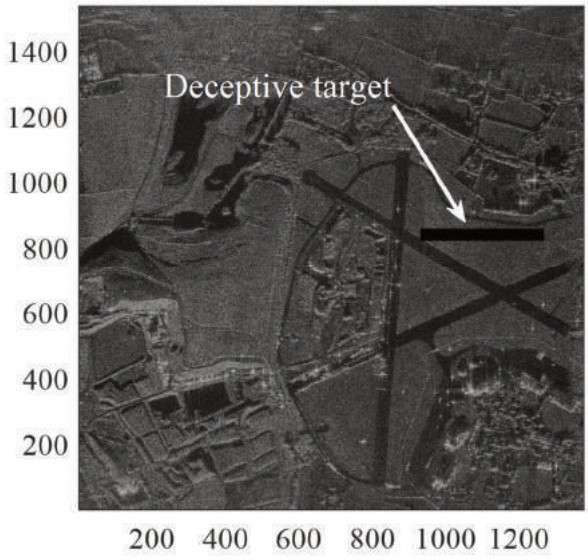

(b) A deceptive horizontal rectangle

Fig. 8 SAR real image plot under deceptive jamming.

In Fig. 9, different SAR images plot under deceptive jamming at different JSR are presented. It is clear that increasing the JSR through Fig. 9a, Fig. 9b, Fig. 9c, and Fig. 9d from [2:8] dB affects the brightness of the deceptive target. The higher JSR, the brighter the deceptive target. Thus, it is very important to choose the JSR value (from the jamming station) in such a way that the deceptive target brightness looks like the real target brightness in the protected scene.

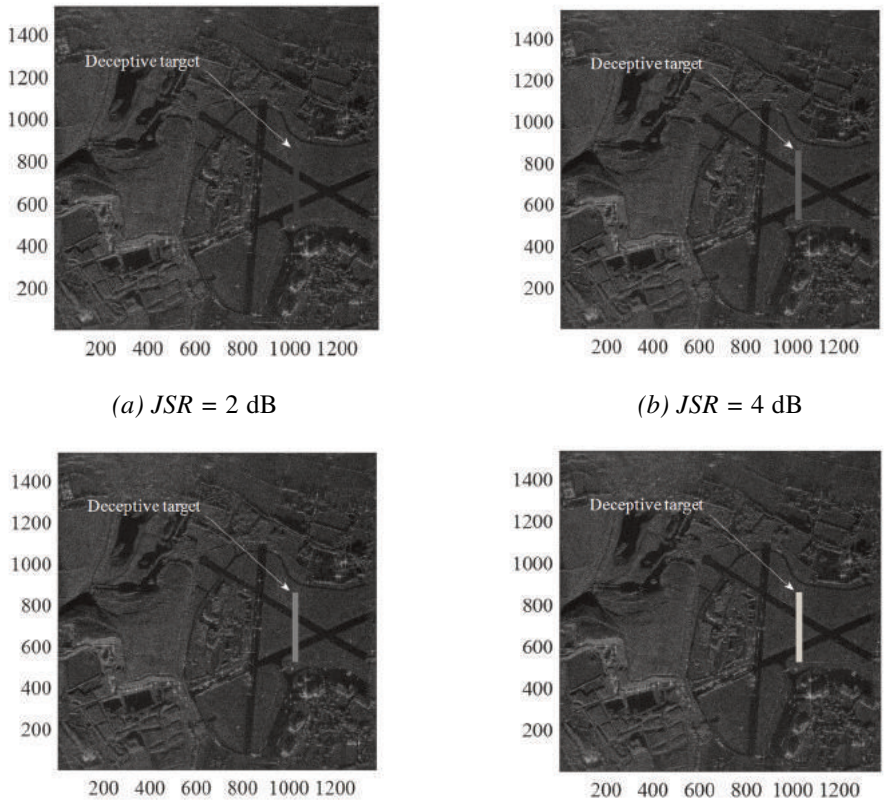

(a) JSR = 2 dB *(b) JSR* = 4 dB

(c) JSR = 6 dB *(d) JSR* = 8 dB

Fig. 9 SAR real image plot under deceptive jamming at different JSR

4.4 JSR Comparison of the Proposed Deceptive Jamming Technique with Other Jamming Techniques

Several amazing notes are obtained by comparing the proposed deception jamming technique results, discussed in this paper, versus the previously published work in this field. There is a significant saving in the jamming power used by the proposed deception technique than other jamming techniques in [5-8]. It is possible to implement the proposed jamming technique in practice rather than the other jamming techniques in [5-8] due to the saving in the jamming power. Fig. 10 shows the comparison of the required jamming power of different jamming techniques in [5-8] to counter SAR.

Different jamming techniques, such as the noise jamming technique in [5], the smart noise jamming in [6], and the complete scene deception in [8] require JSR = 25; 20; 7 dB, respectively, to counter SAR. Meanwhile, the proposed deception jamming requires only JSR = 0 dB to achieve the same jamming effect on SAR.

It is clear that the proposed deception jamming technique required the minimum JSR among other jamming techniques to have the same jamming effect on the protected scene.

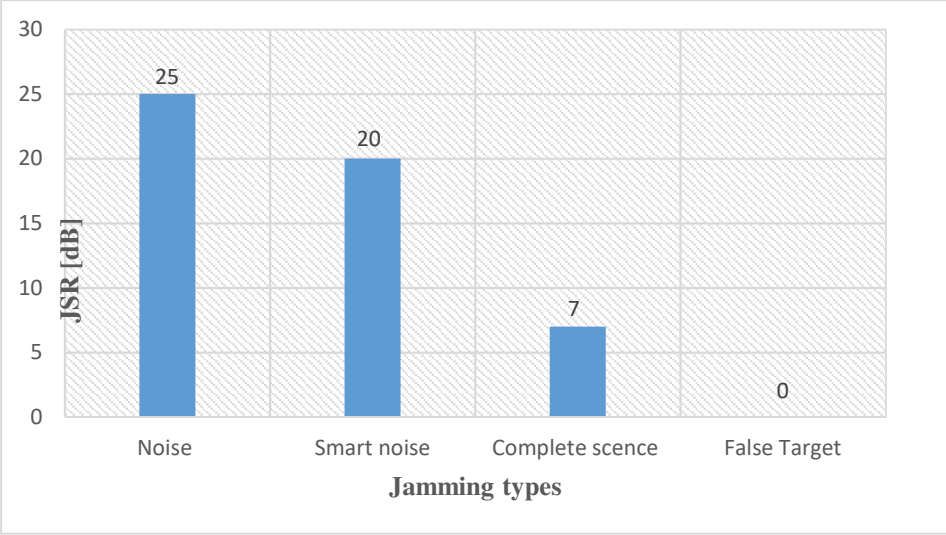

Fig. 10 Comparison of different jamming techniques against SAR.

5 Conclusion

This paper discusses a proposed deceptive jamming technique against SAR by inserting certain object into the SAR focused image with a previously well-known data such as object location and size. The generation of a coherent deceptive jamming signal based on IRDA, its mathematical formula, and its evaluation criteria on SAR are demonstrated. Matlab simulation for SAR point target of deceptive jamming and false target insertion into real large scene are also introduced. MAD is used as an evaluation criterion to measure the deception jamming effect on the SAR model. The higher the values of JSR, the higher the MAD values for both point target deception and false target insertion into large scene.

Different jamming techniques, such as the noise jamming technique in [5], the smart noise jamming in [6], and the complete scene deception in [8] require JSR = 25; 20; 7 dB, respectively, to counter SAR. Meanwhile, the proposed deception jamming requires only JSR = 0 dB to achieve the same jamming effect on SAR. Thus, the proposed deception jamming technique required the minimum JSR among other jamming techniques to achieve the same jamming effect (at the same SNR) on SAR image (the protected scene).

References

[1] JIAGUO, L. Introduction. In: *Design Technology of Synthetic Aperture Radar.* Hoboken: Wiley, 2019, pp. 1-13. ISBN 978-1-119-56454-9.

[2] JIAGUO, L. Radar System Design. In: *Design Technology of Synthetic Aperture Radar.* Wiley-IEEE Press, 2019, pp. 15-73. ISBN 978-1-119-56454-9.

[3] DAI, D., X.F. WU, X. WANG and S. XIAO. SAR Active-Decoys Jamming Based on DRFM. In: *Proceedings of the IET International Conference on Radar Systems.* Edinburgh: IET, 2007, pp. 1-4. ISBN 978-0-86341-848-8.

[4] LIU, Y., W. WANG, X. PAN, L. XU and G. WANG. Influence of Estimate Error of Radar Kinematic Parameter on Deceptive Jamming Against SAR. *IEEE Sensors Journal,* 2016, **16**(15), pp. 5904-5911. DOI 10.1109/JSEN.2016.2570230.

[5] AMMAR, M.A., H.A. HASSAN, M.S. ABDEL-LATIF and S.A. ELGAMEL. Performance Evaluation of SAR in Presence of Multiplicative Noise Jamming. In: *Proceedings of the 34th National Radio Science Conference (NRSC)*. Alexandria: IEEE, 2017, pp. 213-220. DOI 10.1109/NRSC.2017.7893506.

[6] AMMAR, M.A., M.S. ABDEL-LATIF, S.A. ELGAMEL and A. AZOUZ. Performance Enhancement of Convolution Noise Jamming Against SAR. In: *Proceedings of the 36th National Radio Science Conference (NRSC)*. Port Said: IEEE, 2019, pp. 126-134. DOI 10.1109/NRSC.2019.8734626.

[7] AMMAR, M.A. and M.S. ABDEL-LATIF. A Novel Technique for Generation of Multiple Noise Patches on SAR Image. In: *Proceedings of the 12th International Conference on Electrical Engineering (ICEENG)*. Cairo: IEEE, 2020, pp. 277-280. DOI 10.1109/ICEENG45378.2020.9171758.

[8] HANAFY, M., H. HASSAN, M. ABDEL-LATIF and S. ELGAMEL. Performance Evaluation of Deceptive and Noise Jamming on SAR Focused Image. In: *Proceedings of the 11th International Conference on Electrical Engineering ICEENG 2018.* Cairo: Military Technical College, 2018, pp. 1-11. DOI 10.21608/ICEENG.2018.30137.

[9] LIU, Y., T. LI and Z. GU. Research on SAR Active Deception Jamming Scenario Generation Technique. In: *Proceedings of the 5th International Conference on Instrumentation and Measurement, Computer, Communication and Control (IMCCC)*. Qinhuangdao: IEEE, 2015, pp. 152-156. DOI 10.1109/IMCCC.2015.39.

[10] JIAGUO, L. Transmit/Receive Module. In: *Design Technology of Synthetic Aperture Radar.* Wiley-IEEE Press, 2019, pp. 113-159. ISBN 978-1-119-56454-9.

[11] HWANG, J., C. YU and Y. SHIN. SAR-to-Optical Image Translation Using SSIM and Perceptual Loss Based Cycle-Consistent GAN. In: *Proceedings of the International Conference on Information and Communication Technology Convergence (ICTC)*. Jeju: IEEE, 2020, pp. 191-194. DOI 10.1109/ICTC49870.2020.9289381.

[12] JIAO, S. and W. DONG. SAR Image Quality Assessment Based on SSIM Using Textural Feature. In: *Proceedings of the 7th International Conference on Image and Graphics*. Qingdao: IEEE, 2013, pp. 281-286. DOI 10.1109/ICIG.2013.62.

[13] XIONG, Z., R. RADHAKRISHNAN, Y. RUI, A. DIVAKARAN and T.S. HUANG. A Unified Framework for Video Summarization, Browsing, and Retrieval. In: A. BOVIK ed. *Handbook of Image and Video Processing.* 2nd ed. Boston: Academic Press, 2005, pp. 1013-1029. ISBN 978-0-12-119792-1.

[14] SMITH, M.A. and T. CHEN. Image and Video Indexing and Retrieval. In: A. BOVIK ed. *Handbook of Image and Video Processing*. 2nd ed. Boston: Academic Press, 2005, pp. 993-1012. ISBN 978-0-12-119792-1.

[15] WANG, G.X., S.R. PENG, J.J. SUN and H. HE. Effect Evaluation for SAR Suppression Jamming Based on Edge Strength Image. In: *Proceedings of the IET International Radar Conference 2015*. Hangzhou: IET, 2015, pp. 1-4. DOI 10.1049/cp.2015.1016.

[16] JIAGUO, L. Signal Processing. In: *Design Technology of Synthetic Aperture Radar.* Hoboken: Wiley, 2019, pp. 193-247. ISBN 978-1-119-56454-9.

[17] LIN, X., P. LIU and G. XUE. Fast Generation of SAR Deceptive Jamming Signal Based on Inverse Range Doppler Algorithm. In: *Proceedings of the IET International Radar Conference 2013*. Xi'an: IET, 2013, pp. 1-4. DOI 10.1049/cp.2013.0465.

[18] BARLINDHAUG, S., I. HOLM-OLSEN and H. TØMMERVIK. Monitoring Archaeological Sites in a Changing Landscape - Using Multitemporal Satellite Remote Sensing as an 'Early Warning' Method for Detecting Regrowth Processes. *Archaeological Prospection*, 2007, **14**(4), pp. 231-244. DOI 10.1002/arp.307.